ACS SyntheticBiology

Research Article

pubs.acs.org/synthbio

Partitioning Variability of a Compartmentalized *In Vitro* Transcriptional Thresholding Circuit

Korbinian Kapsner[†] and Friedrich C. Simmel*[,†,‡]

[†]Physics Department, TU München, 85748 Garching, Germany

[‡]Nanosystems Initiative Munich, Schellingstrasse 4, 80539 München, Germany

Supporting Information

ABSTRACT: Encapsulation of *in vitro* biochemical reaction circuits into small, cell-sized compartments can result in considerable variations in the dynamical properties of the circuits. As a model system, we here investigate a simple *in vitro* transcriptional reaction circuit, which generates an ultrasensitive fluorescence response when the concentration of an RNA transcript reaches a preset threshold. The reaction circuit is compartmentalized into spherical water-in-oil microemulsion droplets, and the reaction progress is monitored by fluorescence microscopy. A quantitative statistical analysis of thousands of individual droplets ranging in size from a few up to 20 μm reveals a strong variability in effective RNA production rates, which by computational modeling is traced back to a larger-than-Poisson variability in RNAP activities in the droplets. The noise level in terms of the noise strength (the Fano factor) is strongly dependent on the ratio between transcription templates and polymerases, and increases for higher template concentrations.

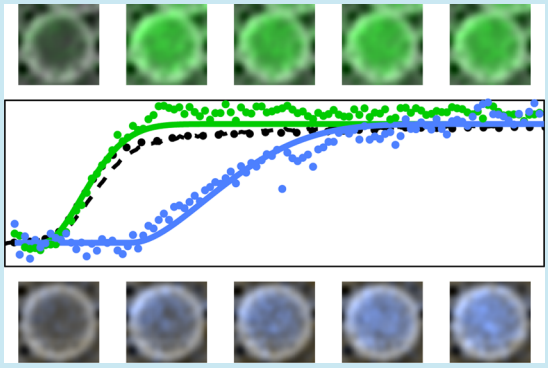

KEYWORDS: *in vitro transcription, genelet circuits, emulsion droplets, stochasticity*

Encapsulation of biochemical reactions into microcompartments is of considerable interest both for fundamental biochemical studies and for technological applications.[1] For instance, compartmentalization into water-in-oil emulsion droplets has been frequently utilized in directed *in vitro* evolution experiments.[2−7] In such experiments, emulsion droplets are used to isolate single genetic mutants from each other, and spatially correlate them with their phenotype. Apart from *in vitro* evolution experiments, emulsion PCR[8−10] is a frequently used technique for the amplification of complex mixtures of genomic DNA, and is nowadays regularly utilized in various sequencing approaches[11] and single cell genomics.[12]

Compartmentalization also is an essential step for the generation of small, cell-like reaction compartments that mimic certain aspects of biological cells. As first steps toward such "artificial cells"[13−15] or "protocells"[16,17] various researchers incorporated genetic components into lipid vesicles.[18−25] Improved protocols now allow researchers to implement increasingly complex functions and behaviors in vesicles. For instance, cell-free gene expression was used to create an artificial cell cortex from the bacterial actin homologue MreB[26] or to implement complex genetic reaction circuits.[27] Recently, also chip-based artificial cellular compartments were realized using lithographic microfabrication methods.[28]

An interesting question of both fundamental and technological importance is the influence of compartmentalization on the dynamics of complex (bio)chemical systems.[29−31] Compartmentalization can affect chemical dynamics in a variety of ways. In sufficiently small volumes, statistical variations in molecule numbers and the stochasticity of chemical processes[32] can become noticeable. Restricted diffusion of chemical species or their transient adsorption to the compartment boundaries[33] can also alter their reaction dynamics. Furthermore, encapsulation itself may affect concentrations and activities of the molecules.[25,34]

Of particular interest in this context is the effect of compartmentalization on the dynamics of nonlinear chemical reaction networks. In the past, various groups studied encapsulation of the Belousov−Zhabotinsky (BZ) oscillator and related oscillating reactions. In these experiments, coupling of the oscillator compartments *via* diffusible oscillator species resulted in various synchronization phenomena[35,36] and even the emergence of Turing patterns.[37,38] In the past few years, also *biochemical* oscillator systems were encapsulated within microdroplets.[39,40] These typically operate at lower concentrations than inorganic chemical oscillators, and their enzymatic components are potentially more sensitive to the encapsulation procedure.[41,42] Compartmentalized biochemical systems are thus expected to display enhanced variability when compared to the inorganic systems.

Our own group has previously studied an *in vitro* biochemical oscillator based on transcription reactions.[40,43,44] The oscillator reaction circuit was comprised of seven DNA species, two RNA

Received: March 19, 2015
Published: May 14, 2015

DOI: 10.1021/acssynbio.5b00051
ACS Synth. Biol. 2015, 4, 1136−1143

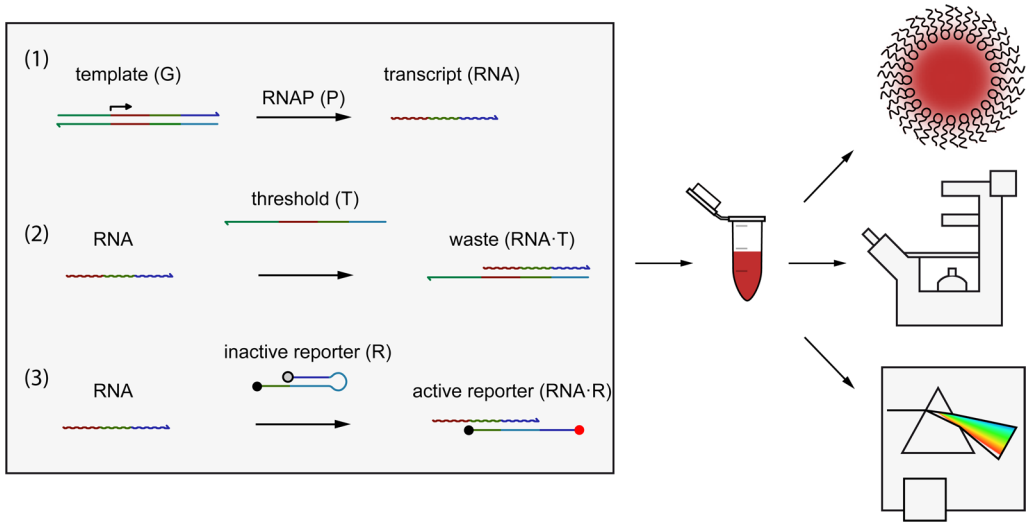

Figure 1. Schematic illustration of the thresholding circuit and our experimental approach: The reaction mix initially contains only four distinct chemical species: T7 RNA polymerase (RNAP), the double-stranded DNA transcription template ("genelet") G, the single-stranded threshold strand T, and hairpin reporter R, which is labeled with a fluorophore (gray/red circle) and a quencher (black circle). (1) RNAP transcribes T (which contains a T7 promoter region) into RNA. Transcribed RNA can then bind to (2) the DNA threshold strand T or to (3) the reporter R. Binding of RNA to the reporter breaks its hairpin structure and thus separates fluorophore from quencher, which results in a strong increase in fluorescence. As it is more favorable for RNA to bind to T, the reporter reaction will be measurably active only when the total concentration of produced RNA exceeds the threshold concentration. Threshold strands can also displace RNA strands from an active RNA-reporter complex, thus deactivating the reporter (not shown). As shown on the right side of the image, the thresholding reaction is characterized using three experimental settings, encapsulated within microemulsion droplets and measured with a fluorescence microscope, in bulk solution on the microscope, and in bulk solution, but measured using a fluorescence spectrometer.

species, and two enzymes, T7 RNA polymerase (RNAP) and RNaseH, which served to produce and degrade the RNA molecules, respectively. In the circuit, two DNA-based transcriptional templates, also termed "genelets",[45,46] were connected in a negative feedback loop, which displayed oscillatory RNA production and degradation dynamics. It was found that encapsulation into small reaction compartments (aqueous emulsion droplets with volumes between 33 fL and 16 pL) resulted in considerable dynamic variability of the oscillator, with increasing variability for smaller volumes. This was traced back to a large variability in enzyme activities, which resulted from the encapsulation procedure. In particular, RNAP appeared to be strongly affected by encapsulation, most probably due to denaturation and aggregation of multiple enzymes,[42,47] while DNA templates were less affected.

In the present study, we investigate the effect of encapsulation on a simple subsystem of the transcriptional oscillator in greater detail, a thresholding circuit composed of only three DNA species and one enzyme (again, RNAP). In this circuit (*cf.* Figure 1) RNA molecules are produced by *in vitro* transcription from a short transcription template. The transcription product can either hybridize to a fully complementary DNA strand, or to a reporter hairpin molecule which is only complementary in part. As binding to the full complement is much more favorable than to the reporter, the complementary strand effectively acts as thresholding device, which absorbs all of the RNA until stoichiometry has been reached between transcripts and the complement. After this point, excess RNA molecules can bind to the doubly labeled sensor hairpin (similar to a molecular beacon,[48] but with a smaller loop, a longer stem and augmented by a toehold sequence), resulting in an ultrasensitive fluorescence response. As explained in more detail below, studying the dynamics of such a thresholding reaction circumvents some of the experimental challenges associated with the exact determination of small molecule numbers in microdroplets.

With respect to our earlier study,[40] we improved our experimental setup, data acquisition, and data analysis procedures. These advances allowed us to analyze much larger numbers of microdroplet compartments, resulting in considerably improved statistics. The lower number of reactant species also enabled a more thorough quantitative analysis of the results, and better comparison with reaction kinetic models. Furthermore, in the experiments we systematically varied the concentration of the genelet templates, while keeping the concentrations of all other species constant. As expected, we found a considerably enhanced variability of the circuits for smaller droplet sizes, reflected in strong variations of the RNA production rate and the "switching time", at which a given threshold concentration is reached by the RNA transcripts. Surprisingly, however, we find the variability to also increase with *increasing* template concentration. This counterintuitive behavior can be explained by a simple model, which considers different partitioning statistics of the genelet templates and RNA polymerases during the generation of the droplets.

RESULTS AND DISCUSSION

Experimental Approach. A schematic overview of the experimental approach taken in this study is shown in Figure 1. After preparation of the thresholding circuit, the reaction mix is quickly emulsified in fluorocarbon oil containing a biocompatible nonionic surfactant[49] using a simple vortexing technique (*cf.* Supporting Information S1.4), which results in microdroplets with a broad size distribution with radii in the range from ≈ 2 μm up to 20 μm. The progress of the reaction in a population of microdroplets is then followed by fluorescence microscopy. As controls, we also monitored the reaction in bulk solution using fluorescence microscopy as well as fluorescence

DOI: 10.1021/acssynbio.5b00051
ACS Synth. Biol. 2015, 4, 1136−1143

spectrometry (*cf.* Supporting Information S2, S3). In all our experiments, the concentration of RNA polymerase ($[P]_0 \approx 100$ *nM*), thresholding strands ($[T]_0 = 600$ nM) and reporter strands ($[R]_0 = 400$ nM) was kept constant, but the concentration of the genelet template $[G]_0$ was systematically varied from 1 nM over 5 nM, 10 nM up to 50 nM. Nucleotide triphosphates (NTPs) were present in excess and did not limit the transcription reactions. Here and in the following, we denote the *total* concentration of a chemical species X by $[X]_0$, and the concentration of *free* X simply by [X].

We specifically focused on the thresholding reaction of Figure 1, as it has a variety of experimental advantages for our study. First, the threshold concentration $[T]_0$ can be conveniently used to create a time delay between the start of the reaction and the initial increase of the signal. This time delay allows for the preparation of a large number of droplets and the subsequent assembly of the microscopic setup. Second, our observable is the rate at which the fluorescence signal rises, which can be determined at a much higher accuracy than the concentrations of the molecular species in the individual droplets. We also preferred the straightforward vortex emulsification over a microfluidic method, as it quickly generates a large range of droplet sizes in a single preparation, including very small droplets, which are hard to produce using microfluidics.

Results of a typical experiment are shown in Figure 2, where the fluorescence time-course of a thresholding reaction is

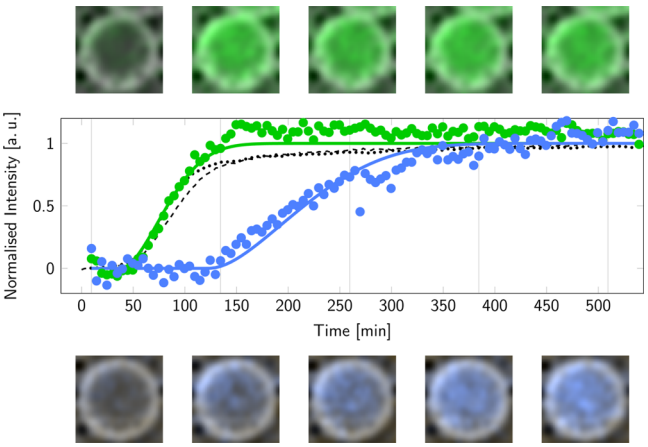

Figure 2. Example of interdroplet variability. The image series on the bottom and the top of the figure are taken from two different droplets (colored green and blue) of the 1 nM-template experiment which display very different production rates. The bulk behavior (black lines, spectrometer data is dashed and microscope data is dotted) is similar to that of the green droplet, but very different from the blue one. The radii of the two droplets are 15.8 and 15.4 μm, respectively.

shown for two equal sized droplets with radius $\rho \approx 16$ μm as well as for the bulk using both microscope and spectrometer measurements. As indicated in the Figure, bulk fluorescence spectrometer and microscopy traces coincide very well. Also some of the droplet-encapsulated circuits show reaction dynamics very similar to the bulk, but we also find large deviations, which become more significant for smaller droplet sizes and which also depend on the concentration ratio of the circuit components.

Data Analysis and Modeling. The reaction scheme shown in Figure 1 corresponds to the following set of chemical equations:

$$\mathrm{P} + \mathrm{G} \underset{k_-}{\overset{k_+}{\rightleftharpoons}} \mathrm{P{\cdot}G} \xrightarrow{k_{\mathrm{cat}}} \mathrm{P} + \mathrm{G} + \mathrm{RNA} \tag{1}$$

$$\mathrm{RNA} + \mathrm{T} \xrightarrow{k_t} \mathrm{RNA{\cdot}T} \tag{2}$$

$$\mathrm{RNA} + \mathrm{R} \xrightarrow{k_r} \mathrm{RNA{\cdot}R} \tag{3}$$

$$\mathrm{RNA{\cdot}R} + \mathrm{T} \xrightarrow{k_x} \mathrm{RNA{\cdot}T} + \mathrm{R} \tag{4}$$

In the additional reaction 4, which is not shown explicitly in Figure 1, threshold strands sequester RNA transcripts prematurely bound to reporter strands. The chemical reactions 1−4 were translated into a set of ordinary differential equations (ODEs) as described in the Supporting Information (SI section S4.1), and numerical solutions to these ODEs were fit to the bulk fluorescence traces obtained for the different template concentrations. From these fits, we determined the RNAP catalytic rate k_{cat} for each set of experiments (*i.e.*, for a given $[G]_0$) individually. This allowed us to account for variations in enzyme activity, which occurred from experiment to experiment, and in particular between different enzyme batches.

In order to analyze circuit variability in the droplets in greater detail, we focused on one characteristic parameter describing the overall dynamics of the circuit, the *RNA production rate* $r = \mathrm{d}[\mathrm{RNA}]_0/\mathrm{d}t$. As a fit of the full reaction scheme to many thousands of droplets per experiment would have been computationally too costly, we analyzed the circuit dynamics using a reduced analytical model. In this model, we make the simplifying assumption that the fluorescence signal equals 0 until the RNA concentration reaches the threshold $[T]_0$. Assuming a constant r this happens at time $t = [T]_0/r$. For $t > [T]_0/r$, newly produced RNA hybridizes with reporter R with an association rate k_r until all of the reporter is activated. This can be translated into the two coupled ordinary differential equations

$$\frac{\mathrm{d}[\mathrm{RNA}]}{\mathrm{d}t} = r - k_r[\mathrm{RNA}][\mathrm{R}] \tag{5}$$

$$\frac{\mathrm{d}[\mathrm{R}]}{\mathrm{d}t} = -k_r[\mathrm{RNA}][\mathrm{R}] \tag{6}$$

which can be solved analytically for [R] (see Supporting Information S5). The normalized fluorescence signal $f(t)$ equals the fraction of *activated* reporters, *i.e.*, $f = [\mathrm{R{\cdot}RNA}]/[\mathrm{R}]_0 = 1 - [\mathrm{R}]/[\mathrm{R}]_0$, and is given by the piecewise defined (but continuously differentiable) function

$$f(t) = \begin{cases} 0 & \text{for } t < \dfrac{[\mathrm{T}]_0}{r} \\ g\left(t - \dfrac{[\mathrm{T}]_0}{r}, r, k_r, [\mathrm{R}]_0\right) & \text{for } t > \dfrac{[\mathrm{T}]_0}{r} \end{cases} \tag{7}$$

where g is given by eq S3.9. In this expression, $[T]_0$ and $[R]_0$ are fixed in the experiments, while the reporter association rate k_r can be extracted from bulk experiments and is found to be $k_r = 8.7 \times 10^2\ \mathrm{M}^{-1}\ \mathrm{s}^{-1}$. Thus, r is the only free parameter and is used to fit $f(t)$ to the data.

In Figure 3, the production rate r normalized by the bulk catalytic rate k_{cat} is compared for the different experimental settings—bulk spectrometer, microscope, and emulsion droplets—for genelet concentrations $[G]_0$ ranging from 1 nM up to 50 nM. Bulk data obtained with the spectrometer or with the microscope agree very well, which indicates that the

DOI: 10.1021/acssynbio.5b00051
ACS Synth. Biol. 2015, 4, 1136−1143

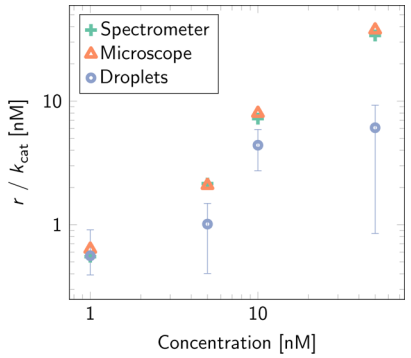

Figure 3. Normalized production rates r/k_{cat} for different template concentrations $[G]_0$. The production rate is obtained by a fit with the simplified reaction model.

microscopic measurement setup *per se* does not introduce any bias into the parameter r (*e.g.*, *via* temperature differences or inhomogeneities, *etc.*). In both cases, bulk production rates increase from $r = 0.22$ nM s^{-1} at $[G]_0 = 1$ nM to $r = 3.4$ nM s^{-1} at $[G]_0 = 50$ nM (r/k_{cat} is in the range 0.6 nM to 34 nM). The determination of r using our fitting procedure was checked to be robust with respect to experimental noise (Supporting Information S6).

If we refer to the standard enzyme kinetic model of eq 1, the RNA production rate r is given by

$$r = \frac{d}{dt}[RNA]_0 = k_{cat}[P{\cdot}G] \tag{8}$$

and thus the normalized production rate r/k_{cat} corresponds to the concentration of active enzyme−substrate complexes $[P{\cdot}G]$. At steady state, this concentration is

$$[P{\cdot}G]_{ss} = \frac{1}{2}([P]_0 + [G]_0 + K_M) \times \left(1 - \sqrt{1 - \frac{4[P]_0[G]_0}{([P]_0 + [G]_0 + K_M)^2}}\right) \tag{9}$$

where $K_M = (k_- + k_{cat})/k_+$ is the usual Michaelis−Menten constant. At small gene template concentrations (for $[G]_0 \ll [P]_0, K_M$), the expression simplifies to (*cf.* also ref 50)

$$[P{\cdot}G]_{ss} \approx \frac{[G]_0}{1 + K_M/[P]_0} \propto [G]_0 \tag{10}$$

As can be seen from Figure 3, for the bulk experiments r/k_{cat} indeed displays a linear dependence on $[G]_0$ (even though $[G]_0 \approx [P]_0, K_M$ for the highest genelet concentrations, $[P]_0 \approx 100$ nM and $K_M \approx 20$ nM in the experiments).

By contrast, the thresholding reactions in the droplets are almost always slower than in bulk. This indicates a loss of activity of some of the RNAPs during encapsulation, which may be caused, *e.g.*, by adsorption at the water/oil interface or by shear flow.[41,42] What is particularly striking is our finding that bulk and droplet experiments in fact agree relatively well for the

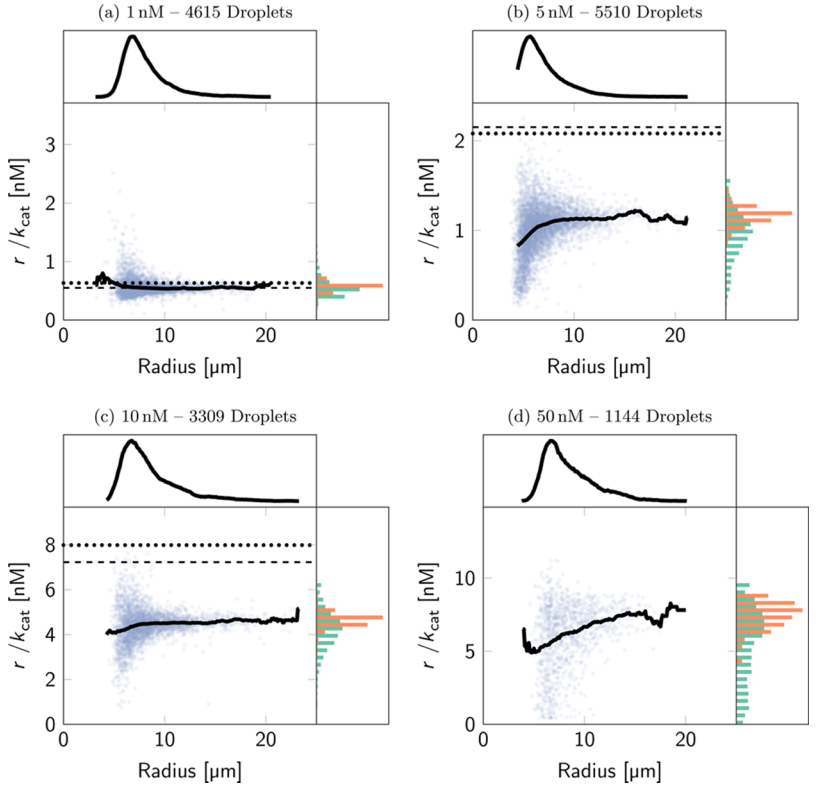

Figure 4. Scatter plots of normalized production rates r/k_{cat} in emulsion droplets for genelet concentrations of (a) 1 nM, (b) 5 nM, (c) 10 nM, and (d) 50 nM. Black dashed lines are the values of the spectrometer measurements. Black dotted lines are the values of the bulk measurement in the microscope (bulk values are not shown in (d) as they differ strongly from the droplet data in this case, *cf.* Figure 3). The solid thick black lines are the average value of 1.5 μm wide moving bins. The curves above the scatter plots in each subgraph represent the relative number of droplets in these bins (*i.e.*, the droplet size distribution). The histograms on the right-hand side are for small droplets (radius <8 μm, green) and larger droplets (radius >12 μm, orange).

DOI: 10.1021/acssynbio.5b00051
ACS Synth. Biol. 2015, 4, 1136−1143

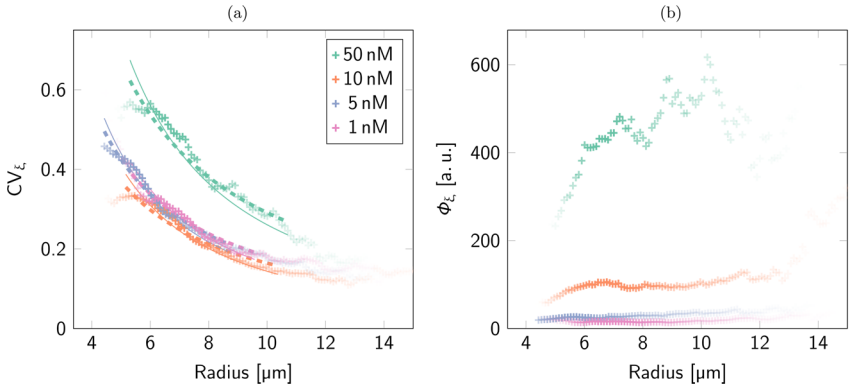

Figure 5. Noise strength $\Phi_\xi = \sigma_\xi^2/\mu_\xi$ calculated for active RNAP-genelet complexes for the different template concentrations. Every data point is calculated for droplets with radii within a bin of width 1.5 μm. In the plots, the opacity of the crosses encodes the statistical significance, *i.e.*, the number of droplets within the radius bin, of the data point. The dashed lines are fits with $a{\cdot}\rho^b$ and the thin solid lines with $a{\cdot}\rho^{-3/2}$, each weighted by the number of droplets in each bin.

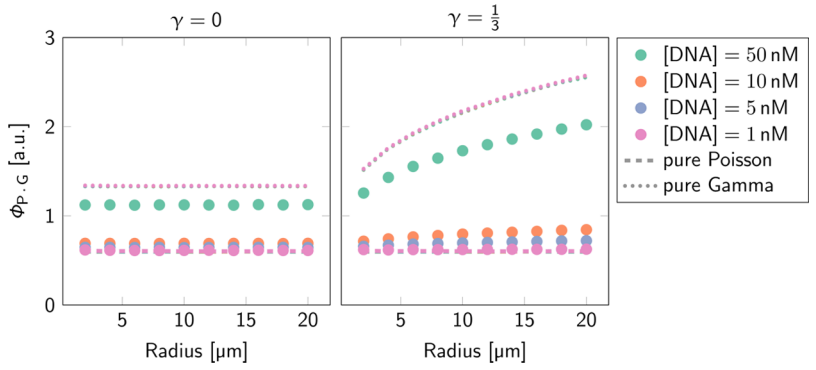

Figure 6. Simulated Fano factor σ^2/μ of rescaled particle numbers ($\Phi_{P\cdot G}$) for the different template concentrations. Before partitioning the system is equilibrated. Then all three molecule species are distributed independently, G and P·G according to a Poisson distribution with a mean value μ that represents the bulk equilibrium and P using a gamma distribution with the appropriate mean μ but with shape parameter $\beta = a{\cdot}\rho^\gamma + b$ ($a = 9$ and $b = 1$ in the figure). The molecule numbers are then equilibrated again within each compartment. The resulting distribution of the P·G particle numbers shows a Fano factor that has a similar radius and template concentration dependency as in the measurement. For comparison, the dashed and dotted lines are generated in simulations, in which all molecule species are distributed either according to Poisson or Gamma statistics. In this case σ^2/μ is almost the same for all four concentrations, and does not display the experimentally observed trend.

smallest template concentration of $[G]_0 = 1$ nM, whereas they systematically differ more strongly for the larger $[G]_0$. At the same time the variance of the production rate also increases with $[G]_0$. At first sight this seems counterintuitive, as due to typical "small number effects" we might have expected larger deviations for the smaller template concentrations (*cf.* analysis below).

Influence of Template Concentration and Droplet Size. We also analyzed the distribution of the production rates r as a function of droplet radius. As can be seen in the scatter plots and histograms shown in Figure 4, the mean production rates deviate from the bulk values more strongly for the smaller droplet radii, and they are also distributed more widely. As already indicated in Figure 3, the width of these distributions appears to be larger for the higher template concentrations. The distributions of the droplet radii themselves are approximately described by log-normal distributions, which is expected for a droplet production process, in which initially large droplets are repeatedly broken down into smaller droplets.[51,52]

As noted above, $r/k_{cat} = [P{\cdot}G]_{ss}$, and we can thus also view the observed variability in the normalized production rate as caused by a variation in the concentration of active enzyme complexes. On the basis of this observation, we further analyzed the variability of our data in terms of typical noise characteristics such as the coefficient of variation $CV_x = \sigma_x/\mu_x$, or the noise strength $\Phi_x = \sigma_x^2/\mu_x$ (also referred to as "Fano factor"), where μ_x is the mean value and σ_x is the standard deviation of the quantity of interest x. Notably, for a Poisson distributed variable $\mu_x = \sigma_x^2$, and thus $\Phi_x = 1$.[53]

For further analysis, we converted the effective concentration of enzyme complexes in each droplet with radius ρ into a quantity ξ proportional to the corresponding number of molecules *via* $\xi = r{\cdot}\rho^3/k_{cat}$. A plot of the resulting noise strength of ξ and its coefficient of variation is displayed in Figure 5. As can be seen in the figure, the dependence of CV_ξ on the radius very well follows a $\propto \rho^{-3/2}$ behavior. As the mean value scales as $\mu_\xi \propto \rho^3$, the observed behavior corresponds to a typical "small number effect" with $CV_\xi \propto \mu_\xi^{-1/2}$. By contrast, in the noise strength Φ_ξ this "trivial" radius/molecule number dependence has been canceled out. Above droplet radii of $\rho \approx 6$ μm, the noise strength appears to be approximately constant, whereas for smaller droplet sizes Φ_ξ seems to become radius-dependent. What is more striking, however, is the variation of noise strength with the template concentration—Φ_ξ increases for larger [G]—which cannot be explained by a simple small number effect alone.

In order to rationalize the trend observed in Figure 5, we computationally modeled several partitioning scenarios, which

DOI: 10.1021/acssynbio.5b00051
ACS Synth. Biol. 2015, 4, 1136−1143

might lead to this peculiar behavior of the noise strength. To generate initial molecule distributions in an ensemble of droplets (assuming that RNA production during droplet generation was negligible), we randomly distributed the molecular species comprising the production part of the thresholding circuit, P, G, and P·G, according to Poisson or gamma distributions, followed by an equilibration step, in which the concentrations were adjusted according to eq 1 (*cf.* Supporting Information S7).

In previous work, we had found that the concentrations of active RNA polymerases partitioned into microemulsion droplets did not follow a simple Poissonian distribution, but could be better described with a gamma distribution, which is given by[40]

$$P(\xi;\,\alpha,\,\beta) = \frac{1}{\beta^{\alpha}\Gamma(\alpha)}\xi^{\alpha-1}e^{-\xi/\beta} \tag{11}$$

Such a distribution can result, *e.g.*, when considering a combination of aggregation and partitioning during the droplet generation process (*cf.* Supporting Information S7.1). For the gamma distribution, the mean value is given by $\mu_\xi = \alpha\beta$, while the variance is var $(\xi) = \alpha\beta^2$. Correspondingly, the coefficient of variation of a gamma distributed variable is $\alpha^{-1/2}$, and its noise strength is equal to β. As shown in Figure 6, if all of the species (*i.e.*, both genelets and enzymes) of the circuit are partitioned into the droplets according to the same distribution, we actually cannot generate any dependence of the fluctuations on the template concentration. The value of β then essentially sets the level of the noise strength of the variables (in Figure 6, $\beta = 1$, corresponding to a Poisson distribution, and $\beta = 10$ are shown). The situation changes if we distribute RNA polymerase according to a gamma distribution ($\beta = 10$), while Poisson partitioning the DNA species and the protein−DNA-complex. In this case, the overall behavior of the noise strength is very well reproduced, suggesting that enzymes and DNA indeed are affected differently by the partitioning process. We note that we actually do not have direct proof for Poisson partitioning of the DNA species (which is here chosen for simplicity) as it is difficult to directly measure nanomolar concentrations (or corresponding molecule numbers) in the droplets using fluorescence microscopy with sufficient accuracy. Our data is consistent, however, with the DNA species being distributed with a smaller variance than the polymerase.

We also attempted to capture the apparent radius dependence of Φ_ξ in our model. It turns out that essentially any assumed dependence of the parameter β on the radius of the droplets is passed through to the noise strength. Specifically, we studied a dependence of the form $\beta(\rho) = a\cdot\rho^{\gamma} + b$ in order to consider potential volume or surface dependent effects exerted during encapsulation of the circuits. In the absence of any radius dependence ($\gamma = 0$, $\beta = const$), the noise strength as a function of radius is (trivially) constant. Interestingly, the radius dependence of Φ_ξ observed for the smaller radii seems more consistent with a scaling of β with a fractional exponent $\gamma < 1$ (*cf.* Figure 6 for the case $\gamma = 1/3$), whereas larger γ do not generate the observed trend. In the Supporting Information (section S7), we speculate on a process that could generate such a behavior. For instance, Φ_ξ and ρ can be coupled by assuming enzyme aggregation to be affected by droplet fission. An exponent $\gamma < 1$ can be produced by assuming that the mean size of the enzyme aggregates becomes smaller in smaller droplets, which will typically have undergone more fissions during the production process.

Overall, the behavior observed in Figure 5 and simulated in Figure 6 shows that a dynamic property such as the production rate r (which in a steady state picture can be related to the concentration of RNAP-genelet complexes [P·G]) can display very different noise characteristics for different "operation points" of our simple circuit. Even though DNA templates are presumably not affected much by the droplet generation and partitioning process, the observed noise strength strongly depends on their initial concentrations. This noise in fact originates from the RNA polymerases, which are present at a *constant* initial concentration, but which *are* affected by droplet partitioning. For $[G]_0 \ll [P]_0$, this can also be qualitatively understood *via* eq 10. It follows that a relative variation in RNA polymerase numbers (or activities) results in a relative variation in $[P\cdot G]_{ss}$, and thus r, which is simply proportional to the enzyme's variation. Therefore, $CV_\xi \propto CV_{\#RNAP}$, independent of the template concentration. This is also reflected by the curves displayed in Figure 5a, which coincide well for the low genelet concentrations. By contrast, eq 10 results in a linear dependence of the noise strength on genelet concentration, *i.e.*, $\Phi_\xi \propto [G]_0$. For larger template concentrations, however, when $[G]_0 \approx [P]_0$, the variable RNAP activity appears to lead to a considerably enhanced variability in RNA production rate.

An important question is whether our observations are specific to the experimental system and preparation method, or whether they have more general validity. It is likely that the exact shape and width of the molecule number distributions depends on experimental factors such as the droplet preparation method or surfactant used.[41,49] For instance, it is conceivable that the rather harsh vortex emulsification leads to particularly strong effects and microfluidic droplets would generate smaller variability. However, previous work on enzyme activities in *small* microfluidic droplets also showed a considerable reduction in activities. Most other work on microdroplets utilized much larger droplets (with diameters ≈100 μm) and concentrations,[39,41] and is thus hard to compare. Regardless of the exact size of the effect, however, it seems likely that different components of a chemical reaction network will be affected differently by compartmentalization, and typically enzymes will be more sensitive than nucleic acid components. Thus, qualitatively we would expect very similar effects also in other experimental settings involving small volumes and molecule numbers.

CONCLUSION

We have quantitatively studied the influence of compartmentalization into microemulsion droplets on the dynamics of a simple *in vitro* transcriptional reaction circuit, which generates an ultrasensitive response when the concentration of an RNA species transcribed from a transcription template reaches a preset threshold. As anticipated from earlier experiments, the circuits display a large variability in their dynamical behavior. This is reflected in widely differing RNA production rates in the droplets, and thus different times at which the threshold is reached. The variability is consistent with the assumption that RNA polymerase activities have a larger-than-Poisson variability in the droplets, while the concentrations of DNA species obey a distribution with much smaller variance than the polymerases (*e.g.*, Poisson). Remarkably this leads to very different noise properties depending on the ratio between transcription templates and RNA polymerases, even though the polymerase concentration is kept constant in our experiments.

DOI: 10.1021/acssynbio.5b00051
ACS Synth. Biol. 2015, 4, 1136−1143

Our results demonstrate that upon compartmentalization, a seemingly simple reaction circuit composed of only three DNA species and one enzyme can display large statistical fluctuations, which, moreover, depend on the exact "operation point" of the circuit. In future experiments, understanding such dependences will be helpful to deliberately operate synthetic reaction circuits in a "noisy" or in a "clean" regime, depending on the application envisioned for these systems. For instance, in genelet circuits enzyme-induced noise is expected to be (relatively) reduced when working at genelet concentrations well below the K_M and [RNAP]. By contrast, our previously investigated transcriptional oscillator was operated at high genelet concentrations ($\approx K_M$, [RNAP]) and thus in the high noise regime.

MATERIALS AND METHODS

Chemicals. The DNA strands were purchased from biomers (Ulm, Germany) and delivered in water with a concentration of 100 μM after HPLC purification. For the formation of the double stranded genelet we mixed the two strands in buffer and anealed them by a 2 h cooling ramp starting at 90 °C and ending at 5 °C. Unless otherwise noticed all chemicals were purchased by Sigma-Aldrich. A list of chemicals and the DNA-sequences can be found in Supporting Information S1.1 and S1.2.

Droplet Production. Water-in-oil emulsion droplets were produced by vigorously shaking the reaction mix with FC-40 Fluorinert oil (F9755, Sigma- Aldrich) that contained 1.8% (weight) of the surfactant E2K0660 (RainDance Technologies). The droplets then were observed on an epifluorescence microscope (Olympus IX71) using ibidi μ-Slides VI$^{0.4}$ as observation chambers.

45 μL oil and 10 μL reaction mix were mixed in a 200 μL tube with a Vortex Genie 2 at maximum speed (2700 Hz) for 30s to 60s. Mixing was performed until the suspension became slightly turbid but not yet milky. This criterion turned out to result in a droplet density that is high enough to allow for observation of a large number of droplets in one image, but which is still low enough to not result in droplet multilayers in the observation chamber.

Microscopy. Video microscopy was performed on an inverted fluorescence microscope (Olympus IX71) using a 10X objective (Olympus UIS2 10× UPlanSApo). For automated microscopy experiments, the microscope was equipped with a filter cube torret (Olympus IX2-RFACA), a motorized probe holder (Prior Scientific), a remote controlled illumination source (consisting of a bright field LED from Prior and a 4-Wavelength fluorescence LED source from Thorlabs (LED4D067 together with DC4104)), and a focus motor (Prior PS3H122). For fluorescence experiments, an RFP filter cube (Ex 530−550 nm/Em 590-∞) was used. Images were recorded with en EM-CCD (Andor LucaR (DL-604 M-#VP)), and automatic video capture was performed with μ Manager 1.4.[54] To enhance the video quality, a software autofocus system was used. During the experiment the probe was kept at 37 °C using a transparent heating plate (TOKAI HIT MATS_UAXKP-D).

Spectrometry. Reference measurements were performed in a fluorescence spectrometer (Cary Eclipse, Varian-Agilent). In these experiments, the reaction mix was put into Hellma precision-cuvettes made from quartz glass SUPRASIL (105.254-QS) and heated to 37 °C by a Peltier block.

Data Analysis. This videos were analyzed by a self-developed MATLAB (Mathworks) program using the image processing toolbox. For further details see Supporting Information S2 and S3.

ASSOCIATED CONTENT

Supporting Information

Materials and methods, experimental details, video and data analysis, computational modeling. The Supporting Information is available free of charge on the ACS Publications website at DOI: 10.1021/acssynbio.5b00051.

AUTHOR INFORMATION

Corresponding Author

*Phone: +49 (0)89 289-11610. Fax: +49 (0)89 289-11612. E-mail: simmel@tum.de.

Notes

The authors declare no competing financial interest.

ACKNOWLEDGMENTS

The authors acknowledge financial support by the DFG Cluster of Excellence Nanosystems Initiative Munich (NIM).

REFERENCES

(1) Theberge, A. B., Courtois, F., Schaerli, Y., Fischlechner, M., Abell, C., Hollfelder, F., and Huck, W. T. S. (2010) Microdroplets in microuidics: an evolving platform for discoveries in chemistry and biology. *Angew. Chem., Int. Ed. 49*, 5846−5868.

(2) Tawfik, D. S., and Griffiths, A. D. (1998) Man-made cell-like compartments for molecular evolution. *Nat. Biotechnol. 16*, 652−656.

(3) Griffiths, A. D., and Tawfik, D. S. (2003) Directed evolution of an extremely fast phosphotriesterase by *in vitro* compartmentalization. *EMBO J. 22*, 24−35.

(4) Paegel, B. M., and Joyce, G. F. (2010) Microuidic compartmentalized directed evolution. *Chem. Biol. 17*, 717−724.

(5) Agresti, J. J., Antipov, E., Abate, A. R., Ahn, K., Rowat, A. C., Baret, J.-C., Marquez, M., Klibanov, A. M., Griffiths, A. D., and Weitz, D. A. (2010) Ultrahigh-throughput screening in drop-based microfluidics for directed evolution. *Proc. Natl. Acad. Sci. U. S. A. 107*, 4004−4009.

(6) Kintses, B., Hein, C., Mohamed, M. F., Fischlechner, M., Courtois, F., Lainé, C., and Hollfelder, F. (2012) Picoliter cell lysate assays in micro uidic droplet compartments for directed enzyme evolution. *Chem. Biol. 19*, 1001−1009.

(7) Ellefson, J. W., Meyer, A. J., Hughes, R. A., Cannon, J. R., Brodbelt, J. S., and Ellington, A. D. (2013) Directed evolution of genetic parts and circuits by compartmentalized partnered replication. *Nat. Biotechnol. 32*, 97−101.

(8) Nakano, M., Komatsu, J., Matsuura, S., Takashima, K., et al. (2003) Single-molecule PCR using water-in-oil emulsion. *J. Biotechnol. 102*, 117−124.

(9) Williams, R., Peisajovich, S. G., Miller, O. J., Magdassi, S., Tawfik, D. S., and Griffiths, A. D. (2006) Amplification of complex gene libraries by emulsion PCR. *Nat. Methods 3*, 545−550.

(10) Schütze, T., Rubelt, F., Repkow, J., Greiner, N., Erdmann, V. A., Lehrach, H., Konthur, Z., and Glökler, J. (2011) A streamlined protocol for emulsion polymerase chain reaction and subsequent purification. *Anal. Biochem. 410*, 155−157.

(11) Metzker, M. L. (2009) Sequencing technologies—the next generation. *Nat. Rev. Genet. 11*, 31−46.

(12) Kalisky, T., and Quake, S. (2011) Single-cell genomics. *Nat. Methods 8*, 311−314.

(13) Pohorille, A., and Deamer, D. (2002) Artificial cells: prospects for biotechnology. *Trends Biotechnol. 20*, 123.

DOI: 10.1021/acssynbio.5b00051
ACS Synth. Biol. 2015, 4, 1136−1143

(14) Noireaux, V., Maeda, Y. T., and Libchaber, A. (2011) Development of an artificial cell, from selforganization to computation and self-reproduction. *Proc. Natl. Acad. Sci. U. S. A. 108*, 3473−3480.
(15) Attwater, J., and Holliger, P. (2014) A synthetic approach to abiogenesis. *Nat. Methods 11*, 495−498.
(16) Luisi, P. L., Ferri, F., and Stano, P. (2006) Approaches to semi-synthetic minimal cells: a review. *Naturwissenschaften 93*, 1−13.
(17) Rasmussen, S. (2009) *Protocells: Bridging Nonliving and Living Matter*, MIT Press, Cambridge, MA.
(18) Fischer, A., Franco, A., and Oberholzer, T. (2002) Giant vesicles as microreactors for enzymatic mRNA synthesis. *ChemBioChem 3*, 409−417.
(19) Monnard, P. (2003) Liposome-entrapped polymerases as models for microscale/nanoscale bioreactors. *J. Membr. Biol. 191*, 87−97.
(20) Hanczyc, M. M., Fujikawa, S. M., and Szostak, J. W. (2003) Experimental models of primitive cellular compartments: encapsulation, growth, and division. *Science 302*, 618−22.
(21) Ishikawa, K., Sato, K., Shima, Y., Urabe, I., and Yomo, T. (2004) Expression of a cascading genetic network within liposomes. *FEBS Lett. 576*, 387−390.
(22) Noireaux, V., and Libchaber, A. (2004) A vesicle bioreactor as a step toward an artificial cell assembly. *Proc. Natl. Acad. Sci. U. S. A. 101*, 17669−17674.
(23) Nourian, Z., Roelofsen, W., and Danelon, C. (2012) Triggered gene expression in fed-vesicle microreactors with a multifunctional membrane. *Angew. Chem., Int. Ed. 51*, 3114−3118.
(24) Nourian, Z., and Danelon, C. (2013) Linking genotype and phenotype in protein synthesizing liposomes with external supply of resources. *ACS Synth. Biol. 2*, 186−93.
(25) Tan, C., Saurabh, S., Bruchez, M. P., Schwartz, R., and Leduc, P. (2013) Molecular crowding shapes gene expression in synthetic cellular nanosystems. *Nat. Nanotechnol.*, 1−7.
(26) Maeda, Y. T., Nakadai, T., Shin, J., Uryu, K., Noireaux, V., and Libchaber, A. (2012) Assembly of MreB filaments on liposome membranes: a synthetic biology approach. *ACS Synth. Biol. 1*, 53−9.
(27) Shin, J., and Noireaux, V. (2012) An *E. coli* cell-free expression toolbox: application to synthetic gene circuits and artificial cells. *ACS Synth. Biol. 1*, 29−41.
(28) Karzbrun, E., Tayar, A. M., Noireaux, V., and Bar-Ziv, R. H. (2014) Programmable on-chip DNA compartments as artificial cells. *Science 345*, 829−832.
(29) Matsuura, T., Hosoda, K., Kazuta, Y., Ichihashi, N., Suzuki, H., and Yomo, T. (2012) Effects of compartment size on the kinetics of intracompartmental multimeric protein synthesis. *ACS Synth. Biol. 1*, 431−437.
(30) Sokolova, E., Spruijt, E., Hansen, M. M. K., Dubuc, E., Groen, J., Chokkalingam, V., Piruska, A., Heus, H. A., and Huck, W. T. S. (2013) Enhanced transcription rates in membrane free protocells formed by coacervation of cell lysate. *Proc. Natl. Acad. Sci. U. S. A. 110*, 11692−11697.
(31) Soga, H., Fujii, S., Yomo, T., Kato, Y., Watanabe, H., and Matsuura, T. (2013) *In vitro* membrane protein synthesis inside cell-sized vesicles reveals the dependence of membrane protein integration on vesicle volume. *ACS Synth. Biol. 3*, 372−379.
(32) Gillespie, D. T. (1977) Exact stochastic simulation of coupled chemical-reactions. *J. Phys. Chem. 81*, 2340−2361.
(33) Fallah-Araghi, A., Meguellati, K., Baret, J.-C., Harrak, A. E., Mangeat, T., Karplus, M., Ladame, S., Marques, C. M., and Griffiths, A. D. (2014) Enhanced chemical synthesis at soft interfaces: a universal reaction-adsorption mechanism in microcompartments. *Phys. Rev. Lett. 112*, 028301.
(34) Zhou, H.-X., Rivas, G., and Minton, A. P. (2008) Macromolecular crowding and confinement: Biochemical, biophysical, and potential physiological consequences. *Annu. Rev. Biophys. 37*, 375−397.
(35) Toiya, M., Vanag, V., and Epstein, I. (2008) Diffusively coupled chemical oscillators in a microfluidic assembly. *Angew. Chem., Int. Ed. 47*, 7753−7755.
(36) Epstein, I., Vanag, V., Balazs, A., Kuksenok, O., Dayal, P., and Bhattacharya, A. (2011) Chemical oscillators in structured media. *Acc. Chem. Res. 45*, 2160−2168.
(37) Vanag, V., and Epstein, I. (2001) Pattern formation in a tunable medium: the Belousov− Zhabotinsky reaction in an aerosol OT microemulsion. *Phys. Rev. Lett. 87*, 228301.
(38) Tompkins, N., Li, N., Girabawe, C., Heymann, M., Ermentrout, G. B., Epstein, I. R., and Fraden, S. (2014) Testing Turing's theory of morphogenesis in chemical cells. *Proc. Natl. Acad. Sci. U. S. A. 111*, 4397−4402.
(39) Hasatani, K., Leocmach, M., Genot, A. J., Estevez-Torres, A., Fujii, T., and Rondelez, Y. (2013) High-throughput and long-term observation of compartmentalized biochemical oscillators. *Chem. Commun. (Cambridge, U. K.) 49*, 8090−8092.
(40) Weitz, M., Kim, J., Kapsner, K., Winfree, E., Franco, E., and Simmel, F. C. (2014) Diversity in the dynamical behaviour of a compartmentalized programmable biochemical oscillator. *Nat. Chem. 6*, 295−302.
(41) Roach, L. S., Song, H., and Ismagilov, R. F. (2005) Controlling nonspecific protein adsorption in a plug-based microfluidic system by controlling interfacial chemistry using fluorous-phase surfactants. *Anal. Chem. 77*, 785−796.
(42) Liu, Y., Jung, S.-Y., and Collier, C. P. (2009) Shear-driven redistribution of surfactant affects enzyme activity inwell-mixed femtoliter droplets. *Anal. Chem. 81*, 4922−4928.
(43) Kim, J., and Winfree, E. (2011) Synthetic *in vitro* transcriptional oscillators. *Mol. Syst. Biol. 7*, 465.
(44) Franco, E., Friedrichs, E., Kim, J., Murray, R., Winfree, E., and Simmel, F. C. (2011) Timing molecular motion and production with a synthetic transcriptional clock. *Proc. Natl. Acad. Sci. U. S. A. 108*, E784−E793.
(45) Kim, J., White, K. S., and Winfree, E. (2006) Construction of an *in vitro* bistable circuit from synthetic transcriptional switches. *Mol. Syst. Biol. 1*, 68.
(46) Kim, J., Khetarpal, I., Sen, S., and Murray, R. M. (2014) Synthetic circuit for exact adaptation and fold-change detection. *Nucleic Acids Res. 42*, 6078−6089.
(47) Maslak, M., and Martin, C. T. (1994) Effects of solution conditions on the steady-state kinetics of initiation of transcription by T7 RNA polymerase. *Biochemistry 33*, 6918−24.
(48) Tyagi, S., and Kramer, F. (1996) Molecular beacons: Probes that fluoresce upon hybridization. *Nat. Biotechnol. 14*, 303−308.
(49) Holtze, C., Rowat, A. C., Agresti, J. J., Hutchison, J. B., Angile, F. E., Schmitz, C. H. J., Koster, S., Duan, H., Humphry, K. J., Scanga, R. A., Johnson, J. S., Pisignano, D., and Weitz, D. A. (2008) Biocompatible surfactants for water-in-fluorocarbon emulsions. *Lab Chip 8*, 1632−1639.
(50) Karzbrun, E., Shin, J., Bar-Ziv, R., and Noireaux, V. (2011) Coarse-grained dynamics of protein synthesis in a cell-free system. *Phys. Rev. Lett. 106*, 048104.
(51) Epstein, B. (1947) The mathematical description of certain breakage mechanisms leading to the logarithmico-normal distribution. *J. Franklin Inst. 244*, 471−477.
(52) Koch, A. (1966) The logarithm in biology 1. Mechanisms generating the log-normal distribution exactly. *J. Theor. Biol. 12*, 276−290.
(53) Thattai, M., and van Oudenaarden, A. (2001) Intrinsic noise in gene regulatory networks. *Proc. Natl. Acad. Sci. U. S. A. 98*, 8614−8619.
(54) Edelstein, A., Amodaj, N., Hoover, K., Vale, R., and Stuurman, N. (2001) *Current Protocols in Molecular Biology*, John Wiley & Sons, Inc., New York.

DOI: 10.1021/acssynbio.5b00051
ACS Synth. Biol. 2015, 4, 1136−1143